Variations in the Conductive and Superconductive Properties of $\{[TiSe_2]_l[NbSe_2]_m\}_n$ Superlattices as a Function of Superlattice Structure

Myungkeun Noh† and David C. Johnson*

Department of Chemistry and Materials Science Institute, University of Oregon, Eugene, Oregon 97403

Greg S. Elliott

Department of Physics, University of Puget Sound, Tacoma, Washington 98416

Received February 22, 2000. Revised Manuscript Received June 22, 2000

An extensive set of $\{[TiSe_2]_l[NbSe_2]_m\}_n$ superlattices has been prepared through controlled annealing of elementally modulated reactants. Electrical conductances were measured from 1.5 K to room temperature. The room temperature conductances are linearly dependent on the number (m) of $NbSe_2$ layers per repeat layer, and independent of the number (l) of semimetallic $TiSe_2$ layers per repeat layer, suggesting that the electronic transport is dominated by the metallic $NbSe_2$ layers. For small l, a positive temperature coefficient of resistance (TCR) is observed, indicative of normal metallic behavior. In general, increasing l reduces the TCR, and for smaller m, the TCR becomes negative at larger l. These samples exhibit a $\sqrt{T}$ temperature dependence to the resistivity variation at low temperatures, characteristic of both weak localization and electron−electron interaction effects for three-dimensional electron flow in strongly disordered systems. Superconducting critical temperatures were also observed to depend strongly on the superlattice structure. A thickness effect is observed in which the transition temperature is decreased as the number of superconducting $NbSe_2$ layers within a repeat layer is reduced. For fixed m, the transition temperature is also reduced as the number of intervening $TiSe_2$ layers is increased, indicating that interlayer coupling is also important. The domained structure of the samples is evident in an unusual $I-V$ behavior observed in the temperature range of the superconducting transition. We interpret this behavior in terms of a simple model based on a patchwork of superconducting domains embedded in normal metal regions.

I. Introduction

A key ingredient in the study of the interrelationships between structure and physical properties of new materials is the "derivative chemistry" that permits a novel structural feature or property to be optimized for detailed study. The layered transition metal dichalcogenides of the Group IVA, VA, and VIA transition metals are an example of a class of materials that have been subject to extensive "derivative chemistry", which has led to a better understanding of the structure−function relationship. The interest in the dichalcogenides resulted from the combination of their highly anisotropic two-dimensional structures and the wide range of interesting electronic and magnetic properties, spanning the range from insulators to metals to superconductors, exhibited by the different members of this family of materials.[1] In addition, the anisotropic two-dimensional structure gives rise to low dimensional electronic instabilities known as charge density waves, which were the focus of much interest in the 1970s and early 1980s.[2,3]

Many synthetic strategies have been used study the interrelationships between structure, composition, and properties of these compounds. The common layered motif of this family of materials results in the ability to systematically vary physical properties by making solid solutions between the binary end members. Varying the annealing temperature results in subtly different structures, polytypes differing in the stacking sequence of the layers or the local coordination of the transition metal between the chalcogen layers.[4] Additionally, the layered structure affords a unique opportunity to systematically vary the physical properties of these materials by the process of intercalation, the insertion of guest atoms, ions, or molecules between the host layers.[5] Typically, redox reactions occur between the guest species and the host lattice that change the density of electronic states of the host lattice. If the interlayer species is magnetic, the resulting compound can be

† Present address: Department of Physics, University of Tennessee, Knoxville, TN 37996.

(1) Wilson, J. A.; Yoffe, A. D. *Adv. Phys.* **1969**, *18*, 193.
(2) Wilson, J. A.; DiSalvo, F. J.; Mahajan, S. *Phys. Rev. Lett.* **1974**, *32*, 882.
(3) Wilson, J. A.; DiSalvo, F. J.; Mahajan, S. *Adv. Phys.* **1975**, *24*, 117.
(4) Brown, B.; Beernsten, D. *Acta Crystallogr.* **1965**, *18*, 31.
(5) Gamble, F. R.; DiSalvo, F. J.; Klemm, R. A.; Geballe, T. H. *Science* **1970**, *168*, 568.

10.1021/cm000159a CCC: $19.00
Published on Web 09/15/2000

either a ferromagnet, an antiferromagnet, paramagnetic, or a spin glass, depending on the host lattice, the concentration of magnetic ions, and the choice of magnetic ion.[6] As a consequence of the wealth of physical phenomena associated with them and the ability to chemically tune these properties, the dichalocogenides have been the focus of numerous papers in the last 30 years.

Over the last 10−14 years there has also been considerable interest in tailoring for physical properties by preparing artificially structured materials.[7,8] These artificially structured materials represent a new "derivative" chemistry prepared using physical synthetic techniques such as molecular beam epitaxy. The ability to create new materials that are structured on the atomic scale has led to novel phenomena when the dimension of the structure is comparable to a characteristic length scale of some underlying physical process. Examples include, but are not limited to, the quantum Hall effect,[9,10] electropic switches based upon quantum confinement of excitonic level,[11] quantized transport in nanostructures,[12] and perpendicular magnetic anisotropy and giant magnetoresistance in magnetic multilayers.[13] The preparation of artificially structured materials has been best developed in the area of semiconductor materials due to their obvious economic importance. The structural quality of artificially structured materials formed in other systems, for example elemental metal superlattices, has not been as high as those prepared from semiconductors. There has been relatively few studies on artificially structured materials involving compounds because the traditional synthesis approaches based on eptiaxial growth become much more difficult as the number of components in the system increases. The preparation of artificially structured materials provides a new avenue for "derivative chemistry", which offers opportunities to discover fundamental new phenomena. One could envision a new chemistry or metallurgy based on design of "composite compounds" if one could rationally prepare such a material and predict its properties from those of the constituents. Adding artificial structuring to the list of "chemical derivative" possibilities provides an additional tool for optimizing properties and correlating properties with structure.

This paper describes the preparation and electrical properties of artificially structured materials containing as components layered transition metal dichalcogenides. The dichaldogenides were partly chosen for the reasons given above and also because earlier epitaxial growth studies by Koma[14] showed that superlattices could be grown with a large lattice mismatch between the components. Dichalcogenide constituents also present the opportunity to prepare superlattices containing compounds with a wide range of physical properties. The constituent compounds chosen in this study, $NbSe_2$ and $TiSe_2$, are a metallic superconductor and a semimetal (or narrow band gap semiconductor), respectively. Both compounds also have charge density wave transitions that are very sensitive to composition and impurity levels.[1,15] We set out to explore the evolution of the electrical properties of a series of these compounds as we separated layers of $NbSe_2$ with increasingly thick layers of $TiSe_2$ by preparing a set of superlattices of the form $\{[TiSe_2]_l[NbSe_2]_m\}_n$, where l and m lie in the range from 1 to 24 and n is chosen so that the films are all about 1000 Å thick. In the first part of this paper, we briefly describe our synthesis approach to preparing these new compounds and our measurement techniques. In the second part of the paper we describe the results of electrical measurements on these new compounds, and we discuss the variation of the magnitude of the conductivity, the superconducting critical temperature, and the temperature dependence of the conductivity as a function of the superlattice structure.

II. Experimental Section

A. Sample Synthesis. Samples were made in a custom-built ultrahigh vacuum chamber with independently controlled sources.[16] Niobium and titanium were deposited at 0.5 Å/s using electron beam guns heaters controlled via a Leybold-Inficon XTC quartz crystal thickness monitors. Selenium was deposited using a Knudsen cell maintained at a constant temperature chosen to maintain a selenium deposition rate of approximately 1.0 Å/s by an Omega CN-9000 temperature-controller, and the rate of selenium deposition was monitored on a quartz crystal thickness monitor. Above each of the sources are computer-controlled shutters to allow precise control of elemental layer thicknesses. The samples were deposited simultaneously on silicon substrates polished to ±3 Å root-mean-square for X-ray studies and on silicon wafers coated with poly(methyl methacrylate) for examining the evolution of the samples free of the substrate.

The preparation of these $\{[TiSe_2]_l[NbSe_2]_m\}_n$ crystalline superlattices has been discussed in detail elsewhere.[17] Briefly, alternating layers of Ti and Se are deposited in the correct composition to form stoichiometric $TiSe_2$ and in the correct absolute amounts to form the desired number (l) of $TiSe_2$ repeat layers. This is followed by deposition of alternating layers of Nb and Se in the correct composition to form stoichiometric $NbSe_2$ and in the correct absolute amounts to form the desired number (m) of $NbSe_2$ repeat layers. This process is repeated until the correct amount of the elements corresponding to the desired number (n) of unit cells of the superlattice is deposited. For each of the component binary compounds, thicknesses of the elements required to obtain the correct composition and desired number of unit cells were determined for three different "building units" as summarized in Table 1. Each building unit resulted in the formation of one, two, or three unit cells of the desired compound from a single deposition of a metal layer followed by a selenium layer. The deposition sequences used to form the samples used in this study along with the measured and calculated repeat unit thicknesses are contained in Table 2.

B. Grazing Angle and High-Angle X-ray Diffraction. X-ray data were collected on a Scintag 2000 $\theta-\theta$ diffractometer

(6) Whittingham, M. S. *Prog. Solid State Chem.* **1978**, *12*, 41−99.
(7) Falco, C. M. *Growth of metallic and metal-containing superlattices*; Dhez, P., Weisbuch, C., Ed.; Plenum Press: New York, 1988; Vol. 182, pp 3−15.
(8) Jin, B. Y.; Ketterson, J. B. *Adv. Phys.* **1989**, *38*, 189−366.
(9) Klitzing, K. v.; Dorda, G.; Pepper, M. *Phys. Rev. Lett.* **1980**, *45*, 494.
(10) Tsui, D. C.; Stormer, H. L.; Gossard, A. C. *Phys. Rev. Lett.* **1982**, *48*, 1559.
(11) Capasso, F. *Physica* **1985**, *129B*, 92.
(12) Devoret, M. H.; Grabert, H.; Grabert, H., Devoret, M. H., Ed.; Plenum: New York, 1992; Vol. 294, pp 1−18.
(13) Fullerton, E. E.; Riggs, K. T.; Sowers, C. H.; Bader, S. D.; Berger, A. *Phys. Rev. Lett.* **1995**, *75*, 330−333.
(14) Koma, A.; Yoshimura, K. *Surf. Sci.* **1986**, *174*, 556−560.
(15) DiSalvo, F. J.; Moncton, D. E.; Waszczak, J. V. *Phys. Rev. B* **1976**, *14*, 4321−4328.
(16) Fister, L.; Li, X. M.; Novet, T.; McConnell, J.; Johnson, D. C. *J. Vac. Sci. Technol. A* **1993**, *11*, 3014−3019.
(17) Noh, M.; Johnson, D. C. *J. Am. Chem. Soc.* **1996**, *118*, 9117−9122.

Table 1. Elemental Layer Thicknesses and the Stoichiometry of Selected Building Units Used To Fabricate the Superlattice Samples

symbol of building unit	final structure after annealing	intended layer thickness (Å)	measured repeat unit thickness (Å)	measured stoichiometry
A_1	1($TiSe_2$)	1.36 5.17	6.5(1)	$TiSe_{1.923}$
A_2	2($TiSe_2$)	2.71 10.35	13.0(3)	$TiSe_{1.980}$
A_3	3($TiSe_2$)	4.07 15.52	20.0(4)	$TiSe_{1.938}$
B_1	1($NbSe_2$)	5.46 1.31	6.7(1)	$NbSe_{2.046}$
B_2	2($NbSe_2$)	10.93 2.62	12.5(3)	$NbSe_{2.006}$
B_3	3($NbSe_2$)	16.39 3.93	20.4(5)	$NbSe_{1.935}$

that has been modified to allow the sample height to be reproducibly adjusted by 0.0002 in. Alignment of the diffractometer was confirmed by checking that the rocking curve maxima due to specular reflection at several angles below $2\theta = 3°$ occurred when the incident and exit angles were equal. Grazing angle X-ray diffraction data were used to confirm the layered structure of the evolving superlattices and analyzed to determine the layer spacing.[18] High-angle diffraction data were used to follow the evolution of crystalline order in the superlattices as a function of annealing temperature and time. The annealing of the samples was done in a drybox with a nitrogen atmosphere with less than 0.2 ppm oxygen.

C. Thermogravimetric Analysis and Differential Scanning Calorimetry. Thermogravimetric analysis was used to determine the actual stoichiometry of the calibration samples containing identical layer thicknesses of the Nb and Se (or Ti and Se) used in the initial ternary superlattice reactants. These samples were heated to 850 °C in flowing air and then held at this temperature for 2 h. The weight change recorded is the difference between mass loss due to the evaporation of excess Se and the weight gain resulting from the oxidation of the niobium forming Nb_2O_5 or titanium to TiO_2, as confirmed by X-ray diffraction.

The heat evolved by diffusion and growth was measured using a Du Pont TA9000 differential scanning calorimetry (DSC) module. Approximately 1 mg of sample free of the substrate was used in this experiment. The sample was heated to 550 °C at a rate of 10 °C/min under flowing nitrogen. This yielded the irreversible changes that occurred during the initial heating. The sample was cooled and reheated at 550 °C two additional times to obtain baselines of the reversible changes in the sample and the cell background. The net heat absorbed or released from the multilayer samples was obtained from the difference between the first and the subsequent runs.

D.Electrical Measurements. For the electrical property study, the dc resistance of a set of $\{[TiSe_2]_l[NbSe_2]_m\}_n$ superlattices was measured using a conventional four-probe technique to eliminate contact resistance. A bridge pattern of identical dimensions was drawn on each of the sample surfaces by using a sharp carbide scriber. Electrical contacts were made to the samples using 0.005 in. diameter copper wires and conductive silver paint. $I-V$ curves were measured at constant temperature to ensure Ohmic behavior and verify the integrity of the contacts. For the temperature-dependent resistance measurements, the samples were mounted on low thermal mass, modular dip sockets and plugged into a mating receptacle in a helium cryostat. Temperature-dependent measurements were made at constant current while the cryostat was cooling slowly. The temperature at the sample was controlled from below 1.5 K to room temperature by adjusting the temperature of the helium gas flowing through the cryostat. The sample temperature was measured using a calibrated Si-diode mounted adjacent to the sample on the cryostat tip.

III. Results and Discussion

A. Annealing Conditions and Structure of $\{[TiSe_2]_l[NbSe_2]_m\}_n$ Superlattices. The as-deposited samples are not crystalline superlattices. Diffraction evidence suggests that they consist of amorphous layers containing small dichalcogenide nuclei at the metal−selenium interfaces. To obtain the desired crystalline superlattice, the samples are annealed at an elevated temperature such that the dichalcogenide nuclei grow but at a temperature low enough that little intermixing of the Ti−Se layers occurs with the Nb−Se layers. The optimal annealing times and temperatures are obtained by following the development of the superlattice diffraction pattern as a function of annealing temperature and time as described in detail previously.[19]

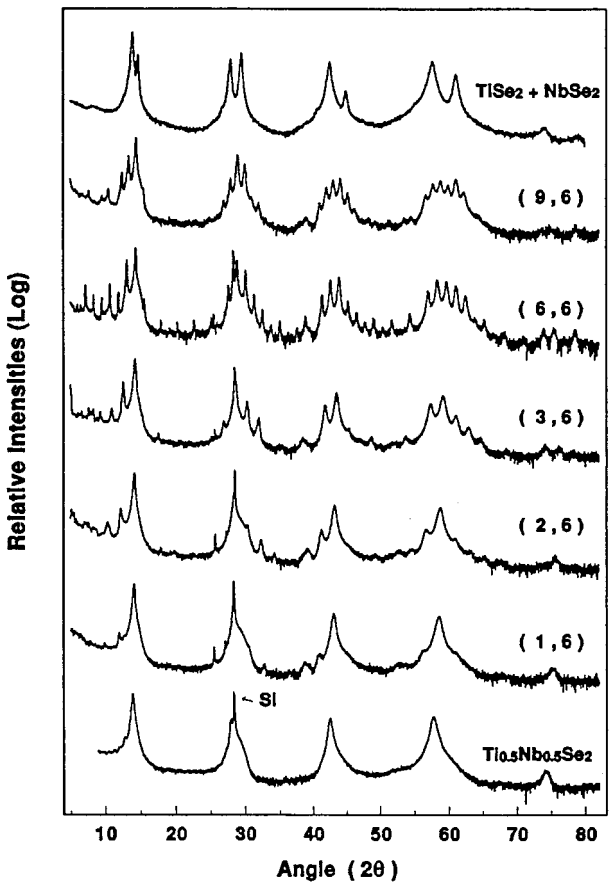

Figure 1. Diffraction data collected for members of the series $[TiSe_2]_l[NbSe_2]_6$. Shown offset for clarity are the diffraction patterns of the homogeneous alloy $NbTiSe_4$ (bottom diffraction pattern), the $l = 1$, 2, 3, 6, and 9 superlattices, and a mixture of the binary compounds (top diffraction pattern).

Representative diffraction patterns of a set of $[TiSe_2]_l[NbSe_2]_6$ samples after annealing are shown in Figure 1. Table 2 contains the designed unit cells of the prepared superlattices, the measured lattice parameters for the superlattices calculated from the diffraction patterns, and the calculated diffraction lattice parameters obtained by adding the unit cells of the components in the designed unit cells. There is good agreement between the measured and calculated superlattice lattice parameters. The structure of a representative sample from this set of samples has been determined in detail using Rietveld refinement.[20] Briefly, the struc-

(18) Novet, T.; Kevan, S.; Johnson, D. C. *Mater. Sci. Eng. A* **1995**, *A195*, 21−27.

(19) Noh, M.; Johnson, D. C. *Ang. Chem.* **1996**, *352666-2669*, 2666−2669.

(20) Noh, M.; Thiel, J.; Johnson, D. C. *Science* **1995**, *270*, 1181−1184.

Table 2. Structures of the Initial Multilayer Reactants and the Repeat Layer Thicknesses for the Initial and Final Structures[a]

unit cell of designed final superlattice	stacking of building units in reactant	measured repeat unit thickness of reactant (Å)	repeat unit thickness of superlattice (Å)	
			measured	calculated
$(TiSe_2)_1(NbSe_2)_6$	$A_1B_3B_3$	47.10(11)	44.09(22)	44.33
$(TiSe_2)_2(NbSe_2)_6$	$A_2B_3B_3$	53.39(13)	50.23(31)	50.38
$(TiSe_2)_3(NbSe_2)_6$	$A_3B_3B_3$	59.40(16)	56.15(40)	56.44
$(TiSe_2)_6(NbSe_2)_6$	$A_3A_3B_3B_3$	78.89(31)	74.16(85)	74.59
$(TiSe_2)_9(NbSe_2)_6$	$A_3A_3A_3B_3B_3$	95.07(11)	92.4(11)	92.75
$(TiSe_2)_1(NbSe_2)_9$	$A_1B_3B_3B_3$	65.69(39)	63.35(35)	63.47
$(TiSe_2)_3(NbSe_2)_9$	$A_3B_3B_3B_3$	78.42(15)	75.16(92)	75.58
$(TiSe_2)_6(NbSe_2)_9$	$A_3A_3B_3B_3B_3$	98.36(42)	93.2(15)	93.73
$(TiSe_2)_9(NbSe_2)_9$	$A_3A_3A_3B_3B_3B_3$	120.62(74)	110.9(17)	111.89
$(TiSe_2)_{12}(NbSe_2)_9$	$A_3A_3A_3A_3B_3B_3B_3$	136.48(28)	129.1(27)	130.04
$(TiSe_2)_3(NbSe_2)_{12}$	$A_3B_3B_3B_3B_3$	100.09(56)	94.23(96)	94.72
$(TiSe_2)_6(NbSe_2)_{12}$	$A_3A_3B_3B_3B_3B_3$	119.98(93)	112.1(17)	112.87
$(TiSe_2)_9(NbSe_2)_{12}$	$A_3A_3A_3B_3B_3B_3B_3$	138.8(10)	130.2(20)	131.03
$(TiSe_2)_{12}(NbSe_2)_{12}$	$A_3A_3A_3A_3B_3B_3B_3B_3$	154.6(30)	148.1(34)	149.18
$(TiSe_2)_6(NbSe_2)_{15}$	$A_3A_3B_3B_3B_3B_3B_3$	138.3(11)	131.2(23)	132.01
$(TiSe_2)_9(NbSe_2)_{15}$	$A_3A_3A_3B_3B_3B_3B_3B_3$	158.19(49)	149.2(29)	150.17
$(TiSe_2)_{12}(NbSe_2)_{15}$	$A_3A_3A_3A_3B_3B_3B_3B_3B_3$	177.6(10)	166.9(27)	168.32
$(TiSe_2)_{15}(NbSe_2)_{15}$	$A_3A_3A_3A_3A_3B_3B_3B_3B_3B_3$	188.6(40)	185.6(33)	186.48

[a] The expected lattice parameter of each superlattice was calculated by adding multiples of the lattice parameters of the binary constituents based on the initial design.

ture of $[TiSe_2]_6[NbSe_2]_6$ contained one mixed metal layer between a block of six $TiSe_2$ layers and four $NbSe_2$ layers. The $NbSe_2$ layers contained 3−5% substitution of Ti for Nb while the $TiSe_2$ layers contained from 5 to 12% Nb substituting for Ti. All of the interlayer and intralayer distances are similar to those of the parent binary compounds. The diffraction patterns of the other samples discussed in this paper can all be reasonably simulated using a similar structural model.

B. Normal State Resistivity of $\{[TiSe_2]_l[NbSe_2]_m\}_n$ Superlattices. The electrical resistance of a set of $\{[TiSe_2]_l[NbSe_2]_m\}_n$ superlattices was measured as a function of temperature as described above. The measured $I-V$ curves were linear at temperatures above the superconducting transition, indicating Ohmic behavior in the normal state. Since bulk $NbSe_2$ is a conductor, whereas bulk $TiSe_2$ is a semimetal, some intermediate behavior might be expected for the composite superlattice. In the superlattice samples the $NbSe_2$ layers have 3−5% titanium substituting for niobium, and the $TiSe_2$ layers contain from 5 to 12% Nb substituting for Ti. While we were unable to find a published study of the electrical properties of the $Nb_{1-x}Ti_xSe_2$ solid solutions, by analogy to results on the $Ta_{1-x}Ti_xSe_2$ solid solution, we anticipate a decrease in the superconducting critical temperature and a suppression of the charge density wave transition with the addition of titanium to $NbSe_2$. Studies of the electrical properties of titanium diselenide samples with a slight excess of titanium $Ti_{1+x}Se_2$ show the rapid suppression of the charge density wave transition with small amounts of added titanium and a transition to metallic behavior.[1,15] The effect of the different electrical character of the $TiSe_2$ and $NbSe_2$ layers in the superlattices can be inferred from the dependence of the measured resistance on the numbers l and m of the individual component layers within a full repeat layer. Since the bulk resistance of a single, uniform sheet is inversely proportional to the thickness of the sheet, it is convenient to use the conductance, G, defined as the inverse of the resistance, R.

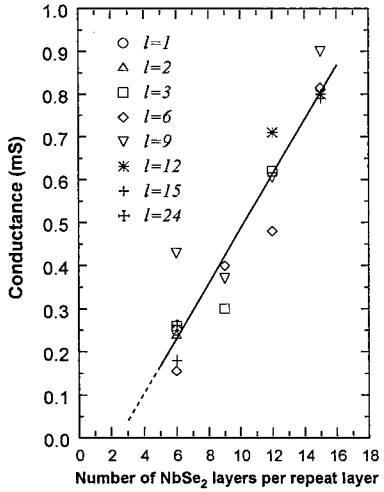

Figure 2. The room-temperature conductance (G) is plotted versus the number (m) of individual $NbSe_2$ layers within a repeat layer of the superlattice, for samples covering a range from 1 to 24 in the number (l) of $TiSe_2$ layers within a repeat layer.

Plotted in Figure 2 is the room-temperature conductance per repeat layer versus the number m of $NbSe_2$ layers. These data are for a set of 16 samples covering a range in the number l of intervening $TiSe_2$ layers, as indicated in the legend. To within some scatter, the conductance increases linearly with increasing $NbSe_2$ layer thickness. Close examination of Figure 2 shows that there is no apparent systematic dependence of the scatter about the line on the number of $TiSe_2$ layers. This implies that the conductance is dominated by the amount of $NbSe_2$ and suggests that the electronic transport is mainly occurring in the metallic $NbSe_2$ layers. The spread in the conductance values between samples with the same number of $NbSe_2$ layers most likely arises from a random variation in the level of static disorder, both within and between crystalline domains. A calculation determines that there is only a 2.0% correlation of the scatter about the best fit line in Figure 4 with the $TiSe_2$ layer thickness. Thus the

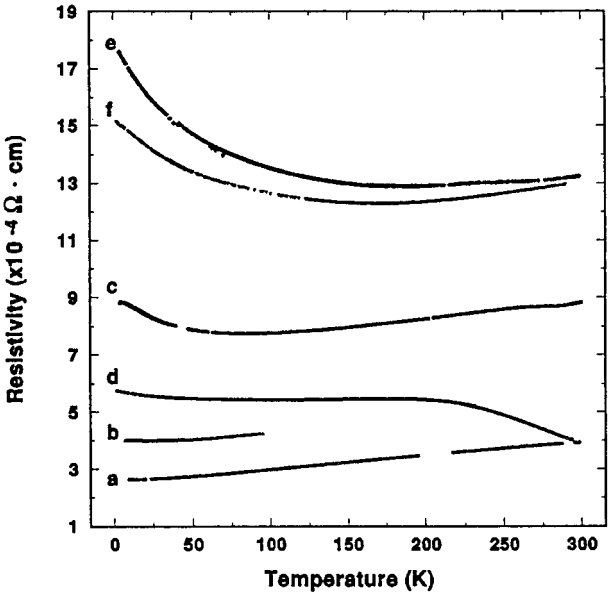

Figure 3. Temperature dependence of the normal state resistivity for $[TiSe_2]_l[NbSe_2]_6$ superlattices with (a) $l = 2$, (b) $l = 3$, (c) $l = 6$, (d) $l = 9$, (e) $l = 15$, and (f) $l = 24$.

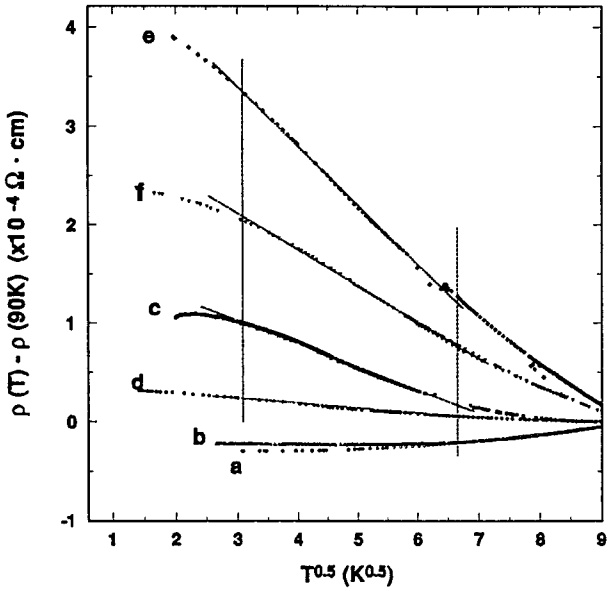

Figure 4. Resistivity variations $\Delta\rho(T) = \rho(T) - \rho(90)$ are plotted versus the square root of the temperature for $[TiSe_2]_l[NbSe_2]_6$ superlattices, with (a) $l = 2$, (b) $l = 3$, (c) $l = 6$, (d) $l = 9$, (e) $l = 15$, and (f) $l = 24$. Only the data below 80 K is shown for clarity. Samples with a negative TCR exhibit a $\sqrt{T}$ dependence in the range from 10 to 40 K.

magnitude of any dependence on the number of $TiSe_2$ layers must be much smaller than the observed level of scatter, and we must look to other experimental quantities to examine the role of the $TiSe_2$ layers.

The slope of a linear best fit to the data, also shown in Figure 2, allows us to calculate a resistivity for the $NbSe_2$ layers of 184 ± 15 $\mu\Omega$ cm. A metallic resistivity of this magnitude typically corresponds to a mean free path on the order of a lattice spacing, leading one to expect that quantum interference effects might play a role in the transport.[21−24] Contributions to the resistivity could include (1) interfacial scattering within the superlattice domains, which could occur in the *c* direction with a mean free path on the order of tens of angstroms, and (2) scattering within the disordered metallic matrix that surrounds the superlattice domains.

Information about the effect of the $TiSe_2$ layers on the normal state electronic transport can be inferred from the temperature dependence of the sample resistivities. Figure 3 shows the temperature dependence of the average sample resistivity for a set of superlattices which all contain six $NbSe_2$ layers per repeat layer, with the number of $TiSe_2$ layers per repeat layer ranging from 2 to 24. The average sample resistivities generally increase as the thickness of the semimetallic $TiSe_2$ block increases, but the overall resistivity value changes very little with temperature in these samples. As noted above, the magnitude of the average resistivity generally increases with the number of $TiSe_2$ layers, simply because a larger fraction of the sample is composed of a more resistive material.

The variations of the resistivity with temperature can be distinguished by three typical behaviors. For samples a and b, the resistivity decreases continuously with decreasing temperature, typical in normal metallic systems. The fractional change in the resistivity over 300 K for the $[TiSe_2]_2[NbSe_2]_6$ sample is about 40%, indicating that scattering from static disorder roughly equals the inelastic scattering contribution at room temperature. For samples e and f, the resistivity decreases slowly as the sample is cooled from room temperature, hits a minimum at around 180 K, and then increases as the temperature drops further. This change in sign in the slope of the curves is characteristic of both semiconducting behavior and of quantum interference effects in highly disordered systems.[21−24] A more complicated temperature dependence is observed for samples c and d, which seems to be an intermediate regime between the two cases mentioned above. The downward deviation clearly observed in the high temperature range of sample d is unique. The well-known quantum interference effects that cause such negative slopes do not usually occur at such high temperatures.[25,26] A possible mechanism for the decrease in the resistivity in sample d is a charge density wave as is found in pure $NbSe_2$. Further experiments, such as transmission electron diffraction measurements, are needed to determine if such a structural phase change actually occurs.

For a better comparison between samples of the resistivity variations with temperature, the change in the resistivity, $\Delta\rho(T) = \rho(T) - \rho(90)$, has been calculated and is shown plotted against $\sqrt{T}$ in Figure 4. By subtracting off the resistivity at a common temperature, the random scatter associated with variable levels of static disorder can be removed. Also, a reference temperature of 90 K is low enough that most of the inelastic

(21) Mott, N. F. *Conduction in Non-Crystalline Materials*; Oxford University Press: New York, 1993.

(22) Lee, P. A.; Ramakrishman, T. V. *Rev. Mod. Phys.* **1985**, *57*, 287.

(23) Dugdale, J. S. *The Electrical Properties of Disordered Metals*; Cambridge University Press: New York, 1995.

(24) Altshuler, B. L.; Aranov, A. G. *electron−electron interactions in disordered systems*; Efros, A. L., Pollak, M., Ed.; Oxford: Amsterdam, 1985; p 1.

(25) Tsuei, C. C. *Phys. Rev. Lett.* **1986**, *57*, 1943.

(26) Kaiser, A. B. *Phys. Rev. Lett.* **1987**, *58*, 1384.

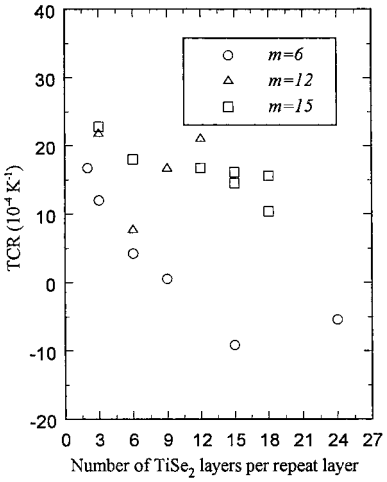

Figure 5. The temperature coefficient of resistance (TCR) at 90 K is plotted versus the number (l) of $TiSe_2$ layers for superlattices with $m = 6$, 12, and 15 $NbSe_2$ layers. A decreasing trend with increasing $TiSe_2$ layers is apparent for the $m = 6$ and $m = 15$ families of samples. For $m = 6$ $NbSe_2$ layers, the TCR changes sign at approximately $l = 6-8$ $TiSe_2$ layers.

scattering contribution will be frozen out. For the samples with thicker intervening $TiSe_2$ layers, labeled c−f, the resistivity falls proportional to $\sqrt{T}$ in the temperature range between 10 and 45 K. The slope of this decrease strongly depends on the sample, showing a larger slope in the samples with a higher $\rho(90)$ value. The $\sqrt{T}$ behavior is characteristic of both weak localization and electron−electron interaction effects for three-dimensional flow in strongly disordered systems.[21−24] Two-dimensional flow yields a logarithmic dependence on temperature; hence, this observation also indicates that the electron transport is not confined solely to $NbSe_2$ layers. Further magnetoresistance measurements need to be performed to investigate the nature and contribution of the quantum interference effects responsible for this observed behavior.[27] The downward deviation from the $\sqrt{T}$ dependence below 10 K is due to superconducting fluctuation effects as the superconducting transition is approached. A similar dependence was observed in Ti−Al alloys by Lin et al.[27] and in the Mo/Si multilayer system by Buchstab et al.[28] These authors showed that in a similar temperature range, a $\sqrt{T}$ dependence can be understood in terms of quantum interference effects.

The effect of the number of $TiSe_2$ layers on the strength of the interaction effects can be quantified by using an appropriate measure of the relative slopes of the curves, as defined by the temperature coefficient of resistance (TCR), $(1/R)/(dR/(dT)$. Figure 5 shows the TCR as a function of the number of $TiSe_2$ layers (l) for the $m = 6$, 12, and 15 families of samples. Data for samples in the $m = 9$ family are missing because they suffered contact problems during temperature cycling. For both the $m = 6$ and $m = 15$ families, there is a clear decreasing trend of the TCR with increasing $TiSe_2$ layer thickness. The change is large for samples with six $NbSe_2$ layers, with a change in sign of the TCR taking place at roughly six to eight $TiSe_2$ layers. The decrease in the TCR is modest for samples in the 15 family, with none of the samples exhibiting a negative TCR. The difference in the rate of decrease of the TCR between these two families is consistent with the difference in their average resistivities, according to a Mooij correlation.[25,26] Samples in the 12 family do not show a consistent trend in the TCR.

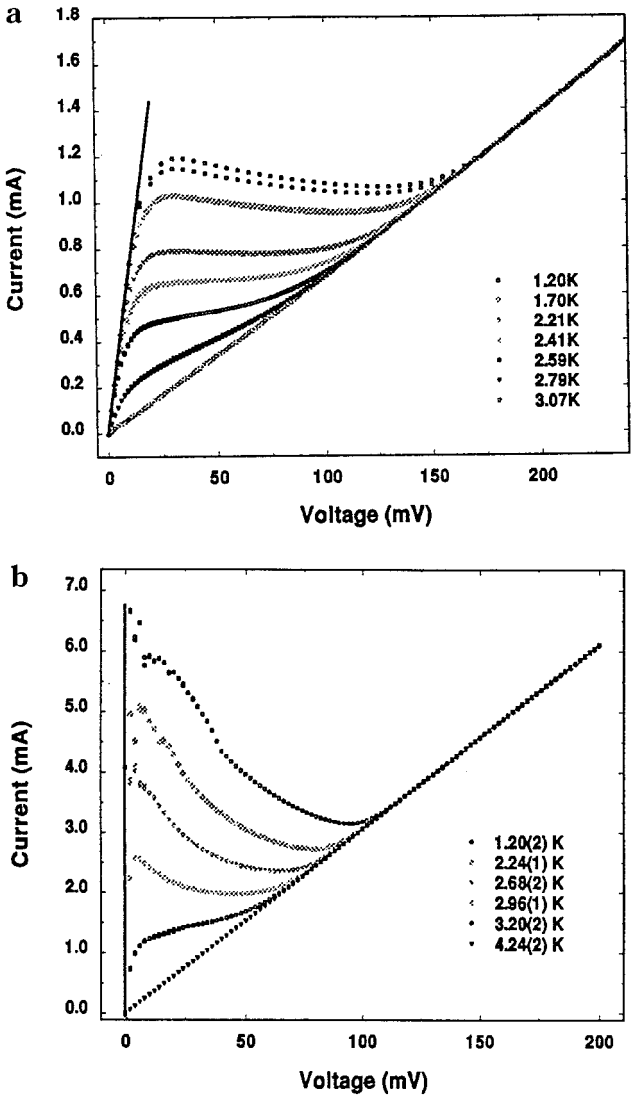

Figure 6. Current−voltage curves at temperatures ranging through the superconducting transition for (a) $[TiSe_2]_9[NbSe_2]_9$ and (b) $[TiSe_2]_{12}[NbSe_2]_{12}$ superlattices. Each curve was obtained at constant temperature by scanning an applied dc voltage and measuring the resulting dc current.

C. Superconducting $I-V$ Characteristics of $[TiSe_2]_l[NbSe_2]_l$ Superlattices. In the initial stage of the synthesis work, a set of superlattices of the form $[TiSe_2]_l[NbSe_2]_l$, $l = 3$, 6, 9, 12, 15, superlattices were prepared. The $I-V$ characteristics of each of these samples were measured in the course of a study of the superconducting properties of the superlattices. In this experiment, unusual $I-V$ behavior was observed in the temperature region between 1.2 K and the superconducting transition temperature T_c. Several isothermal $I-V$ curves for $[TiSe_2]_9[NbSe_2]_9$ and $[TiSe_2]_{12}[NbSe_2]_{12}$ are shown in Figure 6, over a range of temperatures

(27) Rosenbaum, R.; Ben-Shlomo, M.; Goldsmith, S. *Phys. Rev. B* **1989**, *39*, 10009.
(28) Buchstab, E. I.; Butenko, A. V.; Fogel, N. Y.; Cherkasova, V. G.; Rosenbaum, R. L. *Phys. Rev. B.* **1994**, *50*, 10063.

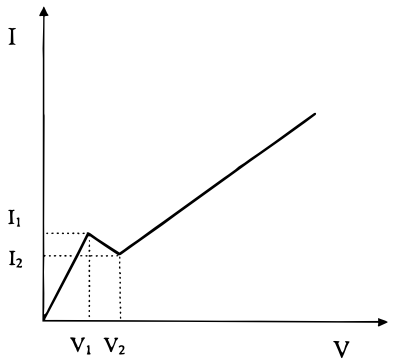

Figure 7. Idealized current−voltage characteristic curve for a granular superconductor, in which the superconducting domains are connected through a surrounding metallic region. The critical currents I_1 and I_2 depend on temperature and separate the different states of the system.

below T_c. These samples were patterned in the standard four-probe measurement configuration, and the $I-V$ curves were obtained at constant temperature by measuring the current flowing through the sample with monotonically increasing voltage bias.

Our interpretation of the observed $I-V$ behavior is based on the known lateral crystalline structure of these superlattices.[29] In our structural model of these samples, there exist superconductor domains that are surrounded by metallic regions. Each superconductor domain has a central area with the correct stoichiometry for the ideal dichalcogenide superlattice. The composition deviates from this stoichiometry toward the periphery of the domains, where there is an excess of transition metal atoms, which diffused out of the domain during crystal growth. For the electronic transport, this "granular" superconductor behaves as a patchwork of interconnected junctions joining superconducting and normal metal regions.

A simplified $I-V$ characteristic for such a system is shown in Figure 7. Under regulated voltage control, the amount of current flowing through the sample is determined by the sample resistance. Ohmic $I-V$ behavior is expected up until a critical voltage, labeled V_1. Below V_1, the crystalline domains stay in the superconducting state and the sample resistance is determined solely by the surrounding metallic region. When the voltage reaches the threshold V_1, the current flowing through the sample begins to exceed the critical current at the periphery of the superconducting domains, where the stoichiometric composition is not ideal. This in turn transforms these areas from the superconducting state to the resistive metallic state. As this transformation proceeds, sample resistance increases and the total current flowing through the sample decreases. This process continues with increasing voltage until all the superconducting areas are converted to the normal metallic phase. Once exhausted, the $I-V$ curve again follows Ohmic behavior, with the current directly proportional to the applied voltage. Figure 8 summarizes the phases of the $[TiSe_2]_9[NbSe_2]_9$ superlattice as a function of temperature and current flowing through the sample.

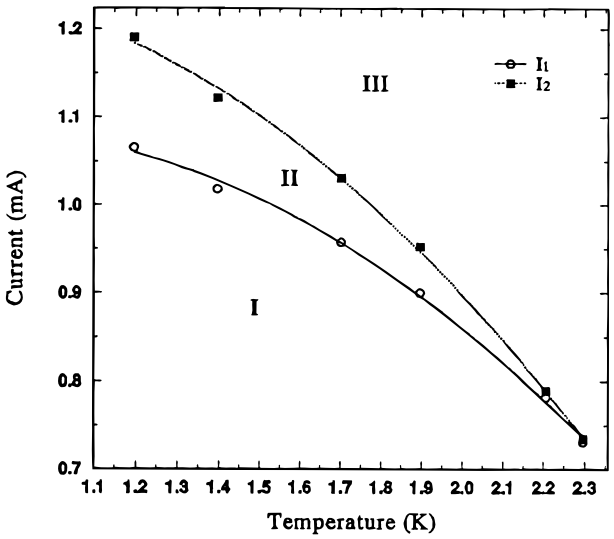

Figure 8. A phase diagram for the $[TiSe_2]_9[NbSe_2]_9$ superlattice as a function of temperature and current flowing through the sample. The regions are separated by the critical currents I_1 and I_2 defined in Figure 7. In region I, superconducting domains are connected through a surrounding metallic region. In crossing region II, the metallic regions increase as superconducting domains shrink. In region III the superconducting domains have all been transformed to metallic regions.

D. Effect of Interlayer Spacing on the Superconducting Transition Temperature. Bulk 2H−$NbSe_2$ is a type II superconductor with T_c at around 7.2 K. The quasi-two-dimensional character of the dichalcogenide superconductor and the role of intercalates between superconducting layers have both been previously studied.[30−32] Frindt has shown that the T_c started to drop significantly as the crystal thickness was reduced below six $NbSe_2$ layers (about 39 Å), and a T_c of 3.8 K was predicted for a single layer.[30] The transition temperature of intercalated dichalcogenide superconductors is known to change with intercalation. In 2H−NbS_2 intercalation lowers T_c from 6 to 2−4 K,[32] while in 2H−TaS_2 intercalation enhances T_c from 0.8 to 2−4 K.[33] In these studies, the separation of the superconducting planes was adjusted by introducing different kind of organic or inorganic molecules. But the resulting variation of T_c with different intercalates cannot be simply compared to each other, because the charge transfer from different intercalates to conducting layers is not the same.

In this experiment, the voltage drop along each $\{[TiSe_2]_l[NbSe_2]_m\}_n$ superlattice was measured as a function of temperature at a constant current of 100 μA. A superconducting transition temperature (T_c) is assigned as the midpoint of the resistance transition, and the width of the transition (ΔT_c) is determined as the temperature difference between the 10% and 90% points on the transition. In Figure 9, the superconducting transition temperatures for samples in the $[TiSe_2]_l[NbSe_2]_6$ and $[TiSe_2]_l[NbSe_2]_{15}$ families are plotted against the number of $TiSe_2$ layers. For samples with six $NbSe_2$

(29) Shin, H. J.; Jeong, K.; Noh, M.; Johnson, D. C.; Kevan, S. D.; Warwick, T. J. *J. Appl. Phys.* **1997**, *81*, 7787−7792.

(30) Frindt, R. F. *Phys. Rev. Lett.* **1972**, *28*, 299.
(31) Thompson, A. H.; Gamble, F. R.; Koehler, R. F. *Phys. Rev. B* **1972**, *5*, 2811.
(32) Hamaue, Y., Aoki, R. *J. Phys. Soc. Jpn.* **1985**, *55*, 1327.
(33) Gamble, F. R.; Osiecki, J. H.; Caia, M.; Pisharody, M.; DiSalvo, F. J.; Geballe, T. H. *Science* **1971**, *174*, 493.

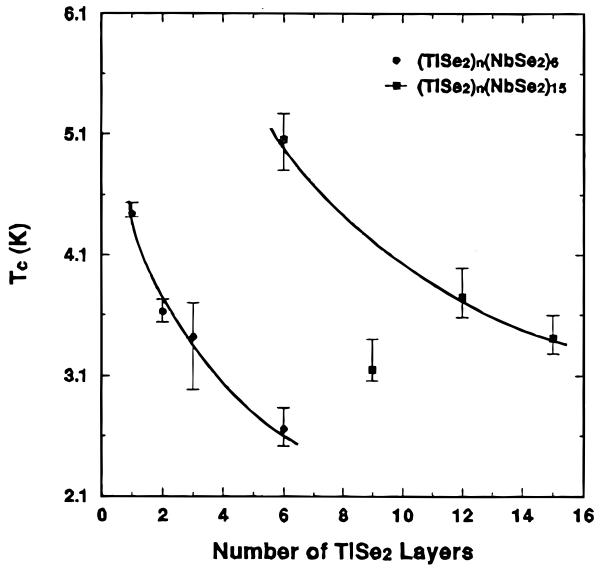

Figure 9. Superconducting transition temperatures are plotted versus the number of $TiSe_2$ layers for members of the $[TiSe_2]_l[NbSe_2]_6$ and $[TiSe_2]_l[NbSe_2]_{15}$ families.

layers, T_c decreases from 4.4 to 2.6 K as the thickness of the intervening $TiSe_2$ block increases from one layer to six layers. For samples with 15 $NbSe_2$ layers, T_c also decreases from 5.1 to 3.4 K as the number of $TiSe_2$ layers increases from 6 to 15.

The observed change of T_c in the $[TiSe_2]_l[NbSe_2]_6$ and $[TiSe_2]_l[NbSe_2]_{15}$ superlattice families can be interpreted as a direct result of different interlayer spacing. Frindt showed that the T_c of six $NbSe_2$ layers was almost same as the bulk value, whereas it was lowered to 4.4 K in this experiment when the layers were separated by a single $TiSe_2$ monolayer.[30] Our experimental results indicate that the T_c of $NbSe_2$ is lowered due to the existence of intervening $TiSe_2$ layers and this shift becomes larger as the separation increases. This experiment also shows that T_c decreases as the thickness of the $NbSe_2$ layer decreases, as seen by comparing data of $[TiSe_2]_6[NbSe_2]_6$ and $[TiSe_2]_6[NbSe_2]_{15}$, which is also consistent with the observation by Frindt.

IV. Summary

The ability to prepare new compounds with controlled superlattice structure provides an additional experimental variable to understand structure−property relationships. We have fabricated a set of $\{[TiSe_2]_l[NbSe_2]_m\}_n$ superlattices by controlled annealing of elementally modulated multilayer reactants. The electrical conductance of these samples has been measured from 1.5 K up to room temperature. The electronic transport appears to be dominated by the metallic $NbSe_2$ component, as evidenced by the dependence of the room-temperature conductance on the number of $NbSe_2$ and $TiSe_2$ layers. The superconducting transition temperature decreases as the thickness of the $NbSe_2$ layers is decreased. The effects of the semimetallic $TiSe_2$ layers can be seen both in the normal state resistivity and in the superconducting transition temperatures. Increasing the number of metallic $TiSe_2$ layers (1) increases the sample resistivity, (2) reduces the TCR in the negative direction, introducing quantum interference effects in samples with thinner $NbSe_2$ layers, and (3) decreases the superconducting transition temperature. The domain structure of the samples is apparent in $I-V$ curves near the superconducting transition temperature. The nonlinear behavior can be understood in terms of a simple model based on a patchwork of superconducting domains embedded in normal metal regions. Further work needed to be done includes magnetoresistance measurements on samples exhibiting a negative TCR, to determine the nature of the quantum interference effects, and low-temperature diffraction measurements on samples which appear to be exhibiting a charge density wave transition

Acknowledgment. The authors would like to thank Martin Wybourne for his useful input and guidance concerning transport in disordered metals. This work was supported primarily by NSF grant DMR-202261 and DMR-203781 at the University of Oregon and through the Murdock Charitable Trust at the University of Puget Sound.

CM000159A